Highly Active Immobilized Catalyst for Ethylene Polymerization: Neutral Single Site Y(III) Complex Bearing Bulky Silylallyl Ligand

Vittoria Chiari, Pascal Rouge, Manel Taam, Pierre-yves Dugas, Gaëlle Pannier, Olivier Boyron, Kai Szeto, Aimery de Mallmann, Christophe Boisson, Mostafa Taoufik

Highly Active Immobilized Catalyst for Ethylene Polymerization: Neutral Single Site Y(III) Complex Bearing Bulky Silylallyl Ligand

Vittoria Chiari,[a,b] Pascal Rouge,[a] Manel Taam,[a] Pierre-Yves Dugas,[a] Gaëlle Pannier,[b] Olivier Boyron,[a] Kai C. Szeto,[a] Aimery de Mallmann,[a] Christophe Boisson,[a,*] Mostafa Taoufik [a,*]

[a] V. Chiari, P. Rouge, M. Taam, P.-Y. Dugas, O. Boyron, K. C. Szeto, A. de Mallmann, C. Boisson, M. Taoufik
Université de Lyon, Université Claude Bernard Lyon 1, CPE Lyon
CNRS, UMR 5128, Catalysis, Polymerization, Processes and Materials (CP2M)
43 Bd du 11 Novembre 1918, 69616 Villeurbanne, France
E-mail: mostafa.taoufik@univ-lyon1.fr, Christophe.boisson@univ-lyon1.fr

[b] V. Chiari, G. Pannier
INEOS Olefins & Polymers Europe, Rue de Ransbeek 310, 1120 Bruxelles, Belgium

Abstract: Exploring the surface organometallic chemistry on silica of highly electrophilic yttrium complexes is a relatively uncommon endeavor, particularly when focusing on tris-alkyl complexes characterized by Y-C σ-alkyl bonds. A drawback with this class of complexes once grafted on silica, is the frequent occurrence of alkyl transfer by ring opening of siloxane groups, resulting in a mixture of species. Herein, we employed a more stable homoleptic yttrium allyl complex bearing bulky η^3-1,3-bis(trimethylsilyl)allyl ligand to limit this transfer reaction. This strategy has been validated by comparing the reactivity between [Y{η^3-1,3-$C_3H_3(SiMe_3)_2$}$_3$] and [Y(o-CH_2PhNMe_2)$_3$] with $SiO_{2\text{-}700}$, where the undesired alkyl transfer reaction occurred for [Y(o-CH_2PhNMe_2)$_3$] leading to a bipodal [(≡SiO)$_2$Y(o-CH_2PhNMe_2)] as major surface species, **2**, while [Y{η^3-1,3-$C_3H_3(SiMe_3)_2$}$_3$] resulted selectively in a monopodal species, [(≡SiO)Y{η^3-1,3-$C_3H_3(SiMe_3)_2$}$_2$], **1**. The materials obtained were characterized by DRIFT, solid state NMR, mass balance analysis and EXAFS. Catalyst **1** showed high activity compared to **2** in ethylene polymerization. The catalytic performance of this neutral catalyst **1** was extended to pre-industrial scale in the presence of hydrogen and 1-hexene. An unprecedented activity, up to 7400 $g_{PE}\cdot g_{cat}^{-1}\cdot h^{-1}$ was obtained even with very low concentration of scavenger Al*i*Bu$_3$ (TIBA/Y = 1.2). The obtained HDPE exhibited desired spherical particle morphology with broad molar mass distribution.

Introduction

Polyolefins represent one of the most important products within chemical industries,[1,2] since the discovery of Ziegler-Natta catalyst for ethylene polymerization about 60 years ago.[3] To date, researches of new and highly active olefin polymerization catalysts still remain actual in both academic and industrial activities.[4–6] For industrial application, heterogeneous catalysts are preferable due to the facile control of the morphologies of the polyolefins which prevents reactor fouling and due to their adaptability for continuous polymerization processes.[7,8] The most common and applied strategy to access heterogeneous olefin polymerization catalysts comprises the immobilization of an organometallic precursor on a solid support functionalized with a co-catalyst. This approach has even been commercialized in particular for group 4 complexes,[9,10] where the co-catalyst is generally based on alkylaluminum or borate, being necessary to generate the highly electrophilic active d^0 cationic species. However, these types of activating supports contain drawbacks like flammable risk and additional cost. Moreover, the active species (cationic d^0 complexes) are extremely reactive and may decompose, thus often resulting in a stability issue for the formulated catalyst. Supported cationic group 4 species are essential due to the high activity in olefin polymerization. Although few examples of MAO- and borate-free activating supports for immobilization of neutral alkyls or hydrides of group 4 species have been reported,[11–13] their activities in ethylene polymerization remain fairly low. The aforementioned issues lead to a necessity to develop highly active and stable catalysts based on neutral transition state metals. An alternative choice is to focus on MAO- and borate-free supported complexes of rare-earth metals. These elements are known to exhibit high intrinsic polymerization activity, even for neutral alkyl (hydrido) metal complexes towards ethylene, without any activator.[14]

Heterogenizing organometallic complexes on solid supports, particularly silica through surface organometallic chemistry (SOMC), has gathered considerable attention in the field of catalysis.[15,16] This approach offers numerous advantages, including enhanced catalyst stability, greater control over catalytic activity and selectivity, and has resulted in the discovery of numerous highly efficient catalytic systems. This concept may have a high potential in polyolefin research as it may offer a direct immobilization of existing homogeneous systems leading to highly stable formulated catalysts. Importantly, these supported single sites essentially serve as pre-formed propagation centers for polymerization reactions. Though silica-supported rare-earth complexes bearing M-C bonds as propagation centers are relatively uncommon,[17–24] further exploration and development in this direction may lead to the discovery of novel catalysts with enhanced activity, selectivity, and stability without any activator, thereby progressing the field of polyolefin research. However, the combination of highly electrophilic rare-earth metal centers and alkyl ligands can lead to ionic M−C bonds that may undergo de-alkylation by ring opening of proximate siloxane bridges, resulting in undesired surface species with low activity.[25,26] This phenomenon may also be a pathway for catalyst deactivation and highlights a significant challenge in the development of silica-supported rare-earth metal catalysts. The reactivity of rare-earth metal centers and the nature of the alkyl ligands must be carefully controlled to mitigate undesired side reactions with the silica support. Approaches to improve the stability of this kind of catalysts by preventing their deactivation are essential for the successful catalytic applications of silica-supported rare-earth

metal complexes. Hence, efforts to design alkyl ligands able to stabilize these complexes once supported on silica are crucial to progress in this field, as well as for the development of more efficient and durable catalytic systems. Indeed, homoleptic tris-alkyl compounds such as $La(CH_2Ph)_3THF_3$ or $La\{CH(SiMe_3)_2\}_3$[27,28] hold significant potential for SOMC approach. These complexes bearing multiple alkyl ligands coordinated to the lanthanum center, exhibit reactivity that can be used for catalytic transformations on solid supports like silica.[25,29] However, only $La(CH_2Ph)_3THF_3$ grafted onto silica dehydroxylated at 700°C ($SiO_{2\text{-}700}$) was reported as a catalyst for ethylene and styrene polymerization.[25] In this case, a transfer of one of the benzyl ligands to the surface with opening of a siloxane bridge has been observed leading to a major bipodal surface species. The latter material was tested in ethylene polymerization and showed low activity.

Recent reports have featured the implication of secondary interactions between rare-earth metals, surface siloxy groups, and their sterically hindered perhydrocarbyl ligands in stabilizing well-defined supported rare-earth metal catalysts on $SiO_{2\text{-}700}$. In fact, it was reported that $Lu[CH(SiMe_3)_2]_3$ reacts with silanols of SiO_{2-700} to give selectively a monopodal surface species, $[(\equiv SiO)Lu[CH(SiMe_3)_2]_2]$ without any secondary alkyl transfer reaction. The characterization of the resulting material $[(\equiv SiO)Lu[CH(SiMe_3)_2]_2]$ by solid-state NMR and EXAFS spectroscopy reveals the presence of secondary Lu···C and Lu···O interactions involving a γ-CH_3 group from the -$CH(SiMe_3)_2$ ligand and a siloxane bridge from the surface, respectively. These interactions show an important role in the stabilization of the metal-ligand fragment on the surface while promoting favorable coordination geometries that avoid an alkyl transfer to silica.[29] Similarly, the reaction of $La[C(SiHMe_2)_3]_3$ with mesoporous silica nanoparticles (SBA-type-MSN) treated at 700 °C, mainly leads to a monopodal $[(\equiv SiO\text{-}La[C(SiHMe_2)_3]_2]$ species and features an average of one bridging La⋯H-Si interaction per alkyl ligand as revealed by solid-state NMR (SSNMR) experiments, including J-resolved Si-H coupling.[20] Nevertheless, these well-defined materials have never been tested in ethylene polymerization.

Based on literature and considering our target to supported monopodal metal bis-alkyl complexes of rare-earth metal for ethylene polymerization, the design of complexes bearing bulky benzyl ligands with strongly coordinating amine or allyl groups seems a promising approach. Specifically, ligands such as o-dimethylaminobenzyl or sterically hindered η^3-1,3-bis(trimethylsilyl)allyl around the metal center could be advantageous for achieving highly stable species on silica dehydroxylated at 700 °C. These allow an access to stable monopodal surface species. We devoted our first study on rare-earth-metal supported complexes to yttrium surface chemistry since this metal is ideally suited for a comparative study because of its midsized Ln^{3+} ionic radius (0.90 Å, for coordination number = 6) allowing to avoid THF-adducts, as reported for complexes $Ln[1,3\text{-}(SiMe_3)_2C_3H_3]_3(THF)$ (Ln = Ce, Nd, Tb).[30] Moreover, accessible homoleptic yttrium complexes with three bidentate benzyl or allyl ligands bound to Y, $[Y(o\text{-}CH_2PhNMe_2)_3]$ and $[Y(\eta^3\text{-}1,3\text{-}C_3H_3(SiMe_3)_2)_3]$, have been reported in literature.[31,32] The immobilization of these complexes allows to compare their structures after reaction with silica surface and their catalytic properties in ethylene polymerization.

In this contribution, we focus on the grafting of homoleptic yttrium complexes, $[Y(\eta^3\text{-}1,3\text{-}C_3H_3(SiMe_3)_2)_3]$ and $[Y(o\text{-}CH_2PhNMe_2)_3]$ on $SiO_{2\text{-}700}$, targeting monopodal organometallic species. The surface structure of the resulting supported complexes has been determined and the structures/properties relationship in ethylene polymerization has been investigated. The most efficient catalyst has further been implemented in ethylene polymerization at pre-industrial scale.

Results and Discussion

Yttrium complexes with η^3-1,3-bis(trimethylsilyl)allyl ligands have recently been largely applied in homogeneous polymerization reaction. The development of such complexes supported on silica for polymerization reaction may provide at least two important advantages: (i) The substantial increase of the size and steric demands of the ligands may further enhance the inertness of the complex and minimize a transfer reaction to silica and provide good solubility in hydrocarbon solvents such as pentane and hexane;[30] (ii) The ability of 1,3-bis(trimethylsilyl)allyl to undergo an interconversion between a bridged (η^3) and a σ (η^1) mode allows to open up coordination sites for α-olefin polymerization without any cationizing agent.[33,34] For all these advantages, we selected a homoleptic complex, $[Y\{\eta^3\text{-}1,3\text{-}C_3H_3(SiMe_3)_2\}_3]$,[32] since we expected that the stability and bulkiness of this complex may limit the transfer of the allyl ligand to silicon by ring opening of siloxane bridges. So, starting from $[Y\{\eta^3\text{-}1,3\text{-}C_3H_3(SiMe_3)_2\}_3]$, our initial goal was to design well-defined monopodal yttrium bis-allyl surface sites bearing a single surface-to-metal bond (**1**, Scheme 1). The homoleptic allylic complex, $[Y(\eta^3\text{-}1,3\text{-}C_3H_3(SiMe_3)_2)_3]$, was first synthesized according to literature procedure reported by Bochmann et al,[32] then grafted on silica dehydroxylated at 700 °C ($SiO_{2\text{-}700}$).

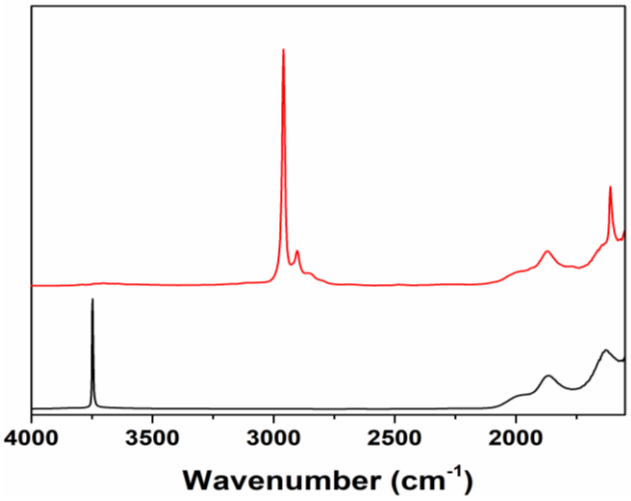

Figure 1. DRIFT spectra of $SiO_{2\text{-}700}$ (black) and after grafting of $[Y\{\eta^3\text{-}1,3\text{-}C_3H_3(SiMe_3)_2\}_3]$ in hexane, 1 (red).

Reaction of $[Y\{\eta^3\text{-}1,3\text{-}C_3H_3(SiMe_3)_2\}_3]$ with silica (Grace silica Sylopol 2408) dehydroxylated at 700 °C ($SiO_{2\text{-}700}$) in hexane (1.6 equivalent per SiOH, see SI) afforded a yellow material, **1**. The

employed silica support featured a specific surface area of 300 $m^2 \cdot g^{-1}$ and showed only non-interacting silanol groups on its surface as evidenced by infrared spectroscopy. (Figure 1, black). After grafting, the DRIFT spectrum of **1** revealed full consumption of the silanols, as shown by the lack of a Si-OH signal at 3747 cm^{-1} (Figure 1, red). New signals at 3000−2885 cm^{-1}, accounting for $\nu(sp^2C-H)$ and $\nu(sp^3C-H)$ of the allylic ligands were also observed. In addition, bands at 1588 cm^{-1} (characteristic for C=C olefin-stretching vibrations) and 1494 cm^{-1} (δ(C−H) vibration of the methylene groups) also appeared. GC analysis of the solution after washing showed the formation of 1,3-bis(trimethylsilyl)propene, $C_3H_4(SiMe_3)_2$. Quantification using tetradecane as external standard gave 0.387 $mmol \cdot g^{-1}$ of $SiO_{2\text{-}700}$, i.e. 0.9 $C_3H_4(SiMe_3)_2$/grafted Y (See SI). The observed C/Y ratio was 17 (th. 18), being consistent with a monopodal surface yttrium species bearing two allyl fragments η^3-$C_3H_3(SiMe_3)_2$, **1** (Scheme 1.).

However, subsequent hydrolysis of **1** yielded 1.5 $C_3H_4(SiMe_3)_2$/Y (0.645 $mmol \cdot g^{-1}$ of $SiO_{2\text{-}700}$), instead of 2 equivalents. The slight deviation might be due to a secondary reaction involving electrophilic substitution of allylic silane released by Y-OH generated during hydrolysis.[35] Solid-state NMR was used to obtain further insight into the structure of **1**. ^{1}H MAS NMR featured broad signals (Figure S1a) at 6.1, 5.6, 1.6 and 0 ppm, accounting for the "central" allylic proton ($Me_3SiCHC\underline{\textit{H}}CHSiMe_3$), vinyl protons ($Me_3SiC\underline{\textit{H}}CHC\underline{\textit{H}}SiMe_3$) and methyl fragments ($\underline{\textit{Me}}_3SiCHCHCHSi\underline{\textit{Me}}_3$) of allyl ligands, respectively. Similar chemical shifts for allylic protons have been reported for the molecular precursor in C_6D_6.[32] The ^{13}C CPMAS NMR spectrum of **1** (Figure S1b) contained a sharp and intense peak at -1.0 ppm assigned to the methyl of the -$SiMe_3$ fragments ($\underline{\textit{Me}}_3SiCHCHCHSi\underline{\textit{Me}}_3$), while the weak and large signals at 93.6 and 161.4 ppm were assigned to the olefinic carbons ($Me_3Si\underline{C}HCH\underline{C}HSiMe_3$) and ($Me_3SiCH\underline{C}HCHSiMe_3$), respectively of the allyl ligands. The ^{29}Si CPMAS NMR spectrum of **1** showed in addition to the expected SiO_2 signal at -103 ppm, one intense peak centered at -8 ppm (Figure 2) assigned to the silicon of -$SiMe_3$ fragment in **1**. Moreover, no evidence of the transfer of an allyl ligand to the silica surface was displayed in ^{29}Si CPMAS NMR spectrum. Indeed, ligand transfer should give a signal characteristic for T3 groups (O_3Si-R) expected around −60 ppm,[36,37] along with the Q-type (SiO_4) signal at −103 ppm. This indicated that no significant η^3-allyl group transferred onto the silica support, contrary to the grafting of the complex bearing a methylene σ-yttrium-carbon bond, $[Y(CH_2SiMe_3)_3THF_3]$ on $SiO_{2\text{-}700}$.[26] Hence, the presence of highly stable η^3-allyl moieties with two bulky substituents (-$SiMe_3$) on carbon bonded to yttrium seemed to prevent the attack of siloxane bridges. silica support, contrary to the grafting of the complex bearing a methylene σ-yttrium-carbon bond, $[Y(CH_2SiMe_3)_3THF_3]$ on $SiO_{2\text{-}700}$.[26] Hence, the presence of highly stable η^3-allyl moieties with two bulky substituents (-$SiMe_3$) on carbon bonded to yttrium seemed to prevent the attack of siloxane bridges.

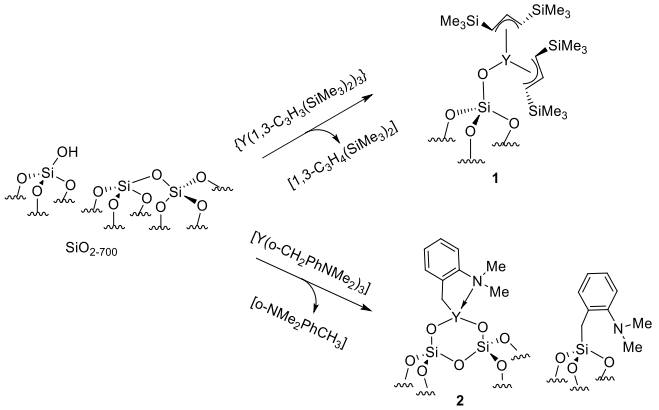

Scheme 1. Grafting of $[Y(o\text{-}CH_2PhNMe_2)_3]$ (**2**) and $[Y\{\eta^3\text{-}1,3\text{-}C_3H_3(SiMe_3)_2\}_3]$ (**1**) on $SiO_{2\text{-}700}$ in toluene or hexane at RT.

The monopodal structure of supported complex **1**, $[(\equiv SiO)Y\{\eta^3\text{-}1,3\text{-}C_3H_3(SiMe_3)_2\}_2]$, was also confirmed by Y K-edge X-ray absorption spectroscopy. The extended X-ray absorption fine structure (EXAFS) fit for the silica-supported species **1** is shown in Figure 3, and the results of the fitting are summarized in Table 1.

The parameter thus extracted from the fits of the EXAFS signals are in agreement with a $[(\equiv SiO)Y\{\eta^3\text{-}1,3\text{-}C_3H_3(SiMe_3)_2\}_2]$ structure on $SiO_{2\text{-}700}$, with ca. one oxygen atoms at 2.15(2) Å and ca. six carbon atoms at 2.58(2) Å. The Y-O distance is longer but still in the range (2.07-2.14 Å) observed by XRD for the three X-type siloxy ligands in $[Y(OSi(OtBu)_3)_3(\eta^2\text{-}HOSi(OtBu)_3)]$ molecular complex[38] and the Y-C distances are close to those observed in $[Y(\eta^5{:}\eta^1\text{-}C_5Me_4SiMe_2NCMe_3)(PMe_3)(\mu\text{-}H)]_2$ (2.542(6)-2.729(7) Å)[39] or calculated by DFT for the average Y-C distance of the $[Y\{1,3\text{-}C_3H_3(SiMe_3)_2\}_3]$ complex (2.574-2.614 Å).[40] Besides, a contribution of second oxygen neighbors, ca. one to two oxygen atoms at 2.35-2.36(2) Å, would be most probably due to surface siloxane bridges. Similar distances were observed for such types of second oxygen neighbors by XRD in $[Y(OSi(OtBu)_3)_3(\eta^2\text{-}HOSi(OtBu)_3)]$ (2.3538(11)-2.5158(10) Å) or by EXAFS (2.40 Å) in the surface species resulting from the grafting of this last complex onto $SiO_{2\text{-}700}$.[38]

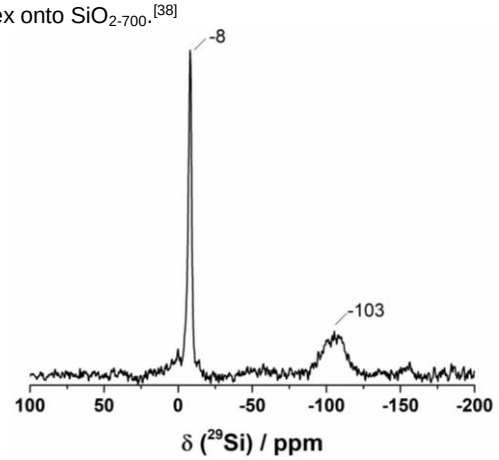

Figure 2. ^{29}Si CPMAS spectrum of **1**.

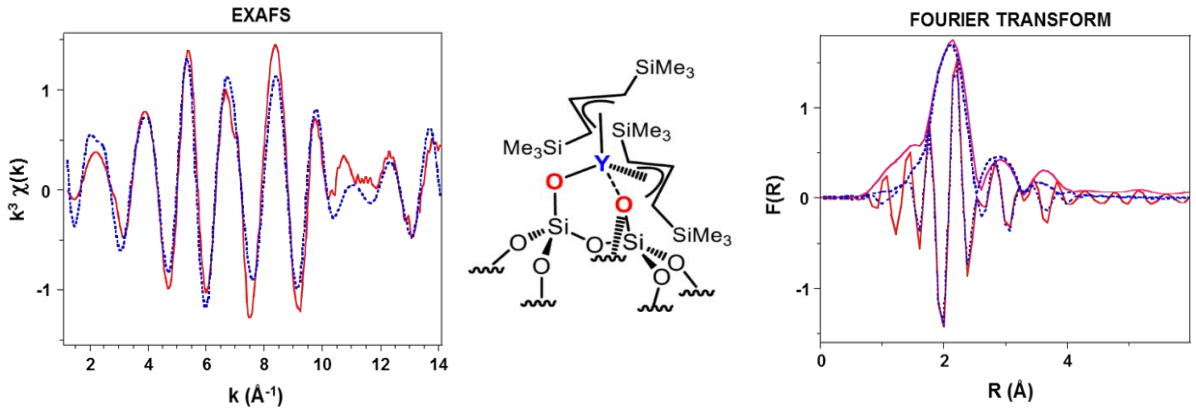

Figure 3. Y K-edge k³-weighted EXAFS (left) and Fourier transform (right) of [Y{η³-1,3-$C_3H_3(SiMe_3)_2$}$_3$]/$SiO_{2\text{-}700}$, **1**. Solid lines: Experimental; Dashed lines: Spherical wave theory. Proposed structure of **1** (middle) according to the EXAFS results.

Table 1. EXAFS parameters for 1[a]. The error intervals generated by the EXAFS fitting program "RoundMidnight" are indicated between parentheses.

Type of Neighbor	Number of Neighbor	Distance (Å)	σ^2 (Å^2)
Y-*O*Si≡	1.1(2)	2.15(2)	0.0056(12)
Y-*C*	5.7[b]	2.58(2)	0.0056[b]
Y---*O*(*Si*≡)$_2$	0.9(4)	2.36(2)	0.0030(27)
Y--*Si*O$_4$	1.1 [b]	3.39(4)	0.0082(35)
Y--*Si*C$_4$	3.8 [b]	3.55(7)	0.042(16)

[a] Δk: [1.3 - 14 Å^{-1}] - ΔR: [0.6-3.9 Å]; S_0^2 = 0.66; ΔE_0 = 5.5 ± 0.9 eV (the same for all shells); Fit residue: ρ = 11.9 %; Quality factor: $(\Delta\chi)^2/v$ = 4.7 (v = 16 / 28). [b] Shell constrained to a parameter above.

The fits could be also improved by adding contributions of further paths, in particular with two types of silicon back-scatters (at 3.39(4) and 3.55(7) Å for **1**), which can be attributed to silicon atoms of X-type siloxy ligands for the shorter distance and to silicon atoms of the (η^3-$Me_3SiCHCHCHSiMe_3$) allyl ligands for the longer distance. Based on these data, the structure of **1** is given in Figure 3.

According to mass balance analysis, DRIFT, solid state NMR and XAS spectroscopies, the complex, [Y{η^3-1,3-$C_3H_3(SiMe_3)_2$}$_3$] reacted selectively with $SiO_{2\text{-}700}$ by protonolysis reaction to give **1**, [(≡SiO)Y{η^3-1,3-$C_3H_3(SiMe_3)_2$}$_2$], as the major surface species. Surprisingly, using the sterically hindered tris-benzyl complex bearing methylene yttrium carbon bond, [Y(o-CH_2PhNMe_2)$_3$], a mixture of mono and bis-grafted surface species **2**, [(≡SiO)Y(o-CH_2PhNMe_2)$_2$] (20%) and [(≡SiO)$_2$Y(o-CH_2PhNMe_2)] (80%) were obtained (Scheme 1).

In fact, $SiO_{2\text{-}700}$ was reacted with an excess of [Y(o-CH_2PhNMe_2)$_3$][31] in toluene at room temperature. The resulting material **2** was characterized by mass balance analysis, surface hydrolysis reaction, as well as DRIFTS (Figure S2). Elemental analysis of **2** indicated Y, N and C loading of 3.82, 1.26 and 9.29 wt%, respectively. The corresponding C/Y atom ratio was 18 and N/Y atom ratio was 2.1. The quantification of N,N-dimethyl-o-toluidine molecule (NNDIMT) released after the grafting reaction using tetradecane as external standard revealed a NNDIMT/Y ratio of 1.2. (See SI). Nevertheless, the quantification of NNDIMT released after the hydrolysis of **2**, indicated only 1.2 o-CH_3PhNMe_2 per yttrium, instead of 2 expected for a monopodal species, **2** [(≡SiO)Y(o-CH_2PhNMe_2)$_2$]. Mass balance analyses on the resulting material, **2**, revealed the formation of a bipodal [(≡SiO)$_2$Y(o-CH_2PhNMe_2)] (80%), **2** as a major species, via protonolysis reaction followed by transfer of one benzyl ligand to the support, even in presence of coordinated amine on Yttrium (Scheme 1). Solid state NMR (^{1}H and ^{13}C) further confirms the ligand transfer phenomenon (Figure S3). ^{1}H MAS NMR showed and intense peak at 7.0 ppm assigned to the aromatic protons. Importantly, the two resolved signals at 2.3 and 2.0 ppm are attributed to Y--N*Me*$_2$ and free N*Me*$_2$ originated from the transferred ligand to silica. However, the Y-C*H*$_2$R (R = $PhNMe_2$), expected at 1.6 ppm is masked by the intense signal attributed to NMe_2.[25] The ^{13}CPMAS NMR also displayed carbon atoms associated to the aromatic ring (120-150 ppm), along with a peak at 68 ppm, assigned to Y-*C*H$_2$R and an intense resonance at 43 ppm due to the amine group (N*Me*$_2$). Furthermore, the weak signal at 20 ppm is attributed to Si-*C*H$_2$R. Such a selective Si–O–Si bridge H opening has already been observed on silica prior to this work in surface organometallic chemistry of main group.[36] Similar results have been recently described by Gauvin and co-workers[25] for the formation of major bipodal species after grafting of benzyl-lanthanide complexes, [La(CH_2Ph)$_3$(THF)$_3$] on $SiO_{2\text{-}700}$. The monopodal catalyst [(≡SiO)Y (η^3-1,3-$C_3H_3(SiMe_3)_2$)$_2$], **1** was investigated in ethylene polymerization (Table S1). In the absence of TiBA scavenger, an activity of 752 g_{PE} $gcat^{-1}$ h^{-1} was measured under 10 bar of ethylene. Under the same conditions, **2** displayed a lower activity of 117 $g_{PE}\cdot g_{cat}^{-1}\cdot h^{-1}$. An increase in activity was noted in the presence of 1-hexene (Table S1) revealing a "comonomer effect", as already observed in literature, for example for Cr/silica (Phillips) catalysts.[41] In fact, the rate of ethylene polymerization was significantly enhanced by the addition of a small amount of α-olefinic co-monomer. This co-monomer effect can be explained by change in the chemistry of the active sites upon coordination of the more electron-rich α-olefin. Interestingly, very high molar masses were measured by SEC analyses together with a broad molar mass distribution.

Indeed, the DSC characterization of these polymers revealed very high melting temperatures for the first heating, 143 °C. Upon second heating the melting temperatures found for the three samples were around 134-135°C with 54-67% of crystalline fraction (Table S1 and Figure S4). This thermal behavior is proper of UHMWPE resins.[42] The use of scanning electron microscopy (SEM) to analyze the morphology of polymers obtained from different polymerization processes provides valuable insights into the structure and characteristics of the resulting materials. The SEM images in Figure 4 revealed spherical particles characteristic of resins produced via heterogeneous slurry polymerization processes.

The transition from lab-scale to industrial-scale is a critical phase in the development of any chemical process. The promising results obtained at the lab-scale, with high activities and desirable polymer characteristics, prompted us to scale-up the current system into pre-industrial scale. Indeed, conducting tests in a 5L autoclave provides a more representative environment with respect to industrial conditions with the possibility to investigate different parameters. Analyzing Table 2, which summarizes the experimental conditions and results of polymerization tests using catalyst **1**, provided valuable insights into how different parameters influence the performance of this specific catalyst. Under mild temperatures and pressures, material **1** showed high activity for ethylene polymerization without the presence of co-monomer (1-hexene) and hydrogen (Run 1, Table 2). An activity of 3750 $g_{PE}\cdot g_{cat}^{-1}\cdot h^{-1}$ was obtained under 10 bar of ethylene and 80 °C. Moreover, the activity profile (Figure 5) extracted from the ethylene consumption as function of time provided important information about the activation step, as well as the stability of the catalyst. It was observed that the activation process in this case required about 25 min before the activity stabilized at about 3830 gPE·gcat-1·h-1 until the end of the run (1 h). Importantly, in the presence of hydrogen during ethylene polymerization (runs 2, 3), a notably different activity profile was observed with an impressive final activity of 5540 $g_{PE}\cdot g_{cat}^{-1}\cdot h^{-1}$ (for 2.6 mol% H_2 in ethylene). Addition of hydrogen dramatically reduced the induction time and a high initial activity (ca. 9000 $g\cdot g_{cat}^{-1}\cdot h^{-1}$) was observed after 5 min compared to run 1 (about 2000 $g\cdot g_{cat}^{-1}\cdot h^{-1}$). However, the presence of hydrogen caused a noticeable deactivation until about 45 min and then the activity curves converged. The final activities (after 1 h) between run 1 (without hydrogen) and run 3 (with 2.6 mol% H2 in ethylene) were fairly close and seemed to be stable, probably due to the formation of the same active sites at steady-state. Thus, the active species of the same pre-catalyst in the absence and presence of hydrogen appeared to be different, as reflected by the difference in the initial step. Three main steps are involved in the polymerization process: the initiation, propagation, and transfer reactions. The cycle starts when one ethylene unit is activated onto the allyl-yttrium fragment of [(≡SiO)Y{η^3-1,3-$C_3H_3(SiMe_3)_2$}$_2$] (Scheme 2).

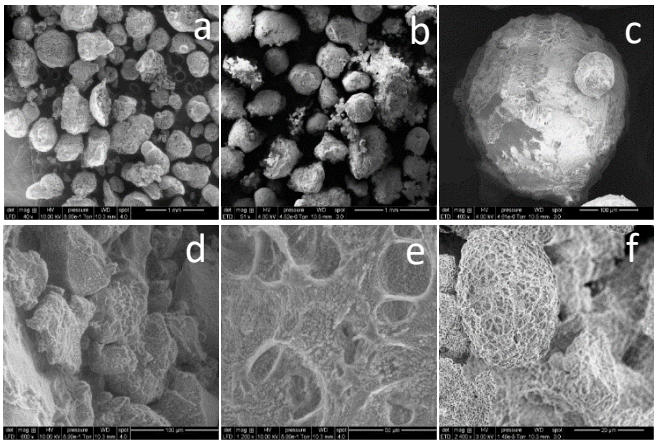

Figure 4. SEM images acquired for the resin obtained with **1** at different magnifications: a) 40x; b) 50x; c) 400x; d) 600x; e) 1200x; f) 2400x.

Table 2. Ethylene polymerization and copolymerization with Y catalyst **1**, at large scale in presence or absence of H_2 and co-monomer.

Run	H_2 in C_2H_4 (mol%)	1-hexene (g)	Yield PE (g)	Activity ($g_{PE}\ g_{Cat}^{-1}\ h^{-1}$)	M_w[d] (Kg mol^{-1})	M_w/M_n[d]	T_m[e] (°C)	Crystallinity[e] (%)
1	0	0	379	3750	N.A.	N.A.	134	56
2	1.3	0	483	4777	617	7.0	135	63
3	2.6	0	554	5540	407	5.8	135	67
4	0	30	460	4600	1393	18	133	62
5[a]	2.6	30	279	2790	339	9.4	134	70
6	2.6	60	222	2220	302	8.7	132	68
7[b]	2.6	30	353	3530	364	9.8	133	67
8[c]	2.6	30	740	7400	262	8.3	133	69

Solvent (Isobutane, 1.5 L), T° = 80 °C, P_{C2H4} = 10 bar, m(**1**) = 100 mg, n(**1**) = 42 μmol, scavenger 0.5 mmol of TiBA, reaction time (1 h). [a] TiBA/Y = 12; [b[TiBA/Y = 6; [c] TiBA/Y = 1.2: [d] Determined by HT-SEC; [e] Determined by DSC.

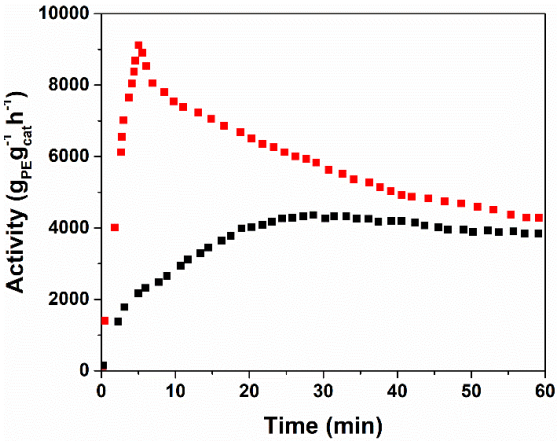

Figure 5. Activity profiles during ethylene polymerization over **1** in presence (red, Run 3, Table 2) and absence of hydrogen (black, Run 1, Table 2).

Thus, the active species of the same pre-catalyst in the absence and presence of hydrogen appeared to be different, as reflected by the difference in the initial step. Three main steps are involved in the polymerization process: the initiation, propagation, and transfer reactions. The cycle starts when one ethylene unit is activated onto the allyl-yttrium fragment of [(≡SiO)Y{η³-1,3-$C_3H_3(SiMe_3)_2$}$_2$] (Scheme 2). A slow activation was observed in the absence of hydrogen, suggesting that the insertion of ethylene into this allyl-yttrium fragment was not energetically and kinetically favorable. The slow rate of this initiation step may be due to a combination of the bulkiness of the trimethylsilyl ligands and the lesser reactivity of the π-allyl ligand towards ethylene insertion compared to a σ-alkyl one (Scheme 2).[43–45] Moreover, Oswald et al.[46] observed that even converting the molecular Y{η³-1,3-$C_3H_3(SiMe_3)_2$}$_3$ complex into the corresponding cationic compound, the activity in ethylene polymerization was very low. Nevertheless, the latter complex, both as neutral or cationic form, efficiently polymerized isoprene, confirming that ethylene insertion into yttrium allyl fragment was unfavorable compared to dienes.[44–46] In the presence of hydrogen, the initial Y-allyl fragment is converted into a Y-H by hydrogenolysis reaction, as shown by Okuda et al.[47,48] The ethylene insertion was then more favorable in a Y-H bond, leading to a higher initial activity in ethylene polymerization for Run 3 compared to Run 1, without H_2 in the feed. A short screening of the hydrogen concentration revealed that 2.6 mol% of hydrogen in ethylene gave the most promising results (Run 3).

Besides, the catalyst deactivation observed in the presence of hydrogen might be attributed to a transformation of the initial monopodal species into bipodal species (Scheme S1). In fact, monopodal species with a Y-CH_2PE fragment, obtained after insertion of ethylene, may be converted into a bipodal [(≡SiO)$_2$Y-R] (R = Alkyl or PE) species after ring opening of silvoxane bridges. This phenomenon was also observed in literature and in this work during the grafting of [Y(*o*-CH_2PhNMe_2)$_3$], **2**, on $SiO_{2\text{-}700}$ (*vide supra*) when the alkyl ligands with Y-CH_2R (R = Ph, o-NMe_2Ph, $SiMe_3$) fragments were employed.[25,26] The occurrence of a gradual ligand transfer was supported by the activity profile (Figure 5) where in Run 1 and Run 3 the same activity is reached at the end of the polymerization experiment (1 h).

In large scale polymerization, the "co-monomer effect" was also observed, as justified by comparison of Run 1 and Run 4. On the other hand, addition of co-monomer (1-hexene) in the presence of 2.6 mol% of hydrogen in ethylene resulted in a decrease of the activity (Run 5 and 6), thus no simultaneous beneficial effect of both hydrogen and 1-hexene was observed. It is known for electron rich Cp_2LnH that the corresponding allyl complex can be formed in contact with an α-olefin,[34,49] like 1-hexene. Such rare-earth allyl fragments have been experimentally proven to be more robust and resistant towards ethylene insertion.[46] However, the presence of Y-allyl in this case was less likely since this fragment will be immediately hydrogenated by a constant supply of H_2 in the environment,[34,49] as also observed in Run 3. Moreover, it has been reported that higher temperatures favor olefin insertion rather than the competing allylic C-H activation and η^3 allyl formation.[49] Thus, in this particular case (Run 5 and 6), hydrogenation of olefins over the extremely active Y-H site most likely occurred,[50] causing a substantial neutralization of H_2 and 1-hexene by consumption. In the absence of hydrogen and 1-hexene, obtaining accurate measurements of the molar masses of the polymers produced with catalyst **1** (Run 1) was challenging due to their ultra-high molecular weight nature. However, when 1-hexene was introduced (Run 4), a linear polyethylene with high molar masses (M_w = 1393 kg mol^{-1}) and a broad molar mass distribution was observed. The decrease of molar masses can be easily explained by the well-known mechanism of chain transfer to hexene, leading to a vinyl-terminated chain and the formation of a Y-hexyl species. Since hydrogen acts as a transfer agent, its presence has made it possible to control the molar mass of polyethylene, as shown in Table 2. DSC characterization of these polymers revealed that the melting temperatures lied around 132-135 °C for all samples with 57-67% crystalline fraction (Table 2).

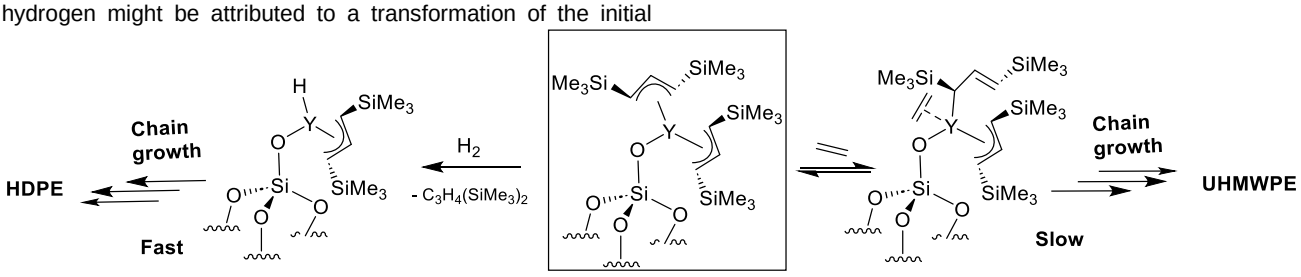

Scheme 2. Initiation steps during ethylene polymerization with **1** in presence and absence of hydrogen.

Finally, the concentration of the scavenger (TiBA) was investigated. As indicated in Table 2, the activity increased considerably when the concentration of TiBA was reduced to TiBA/Y = 1.2. This result indicated that the alkylaluminum in presence of H_2 and 1-hexene interacted with the active species, possibly forming heterobimetallic surface species, thereby reducing the concentration of active sites available for the polymerization reaction for high TiBA/Y ratios (TiBA/Y = 6 or 12).[2,32,51–53] Moreover, catalyst **1**, even bearing yttrium neutral sites, demonstrated unprecedented activity among supported rare-earth catalysts in the field of ethylene polymerization, reaching an activity of up to 7400 $g_{PE}\cdot g_{cat}^{-1}\cdot h^{-1}$. Indeed, this corresponds to an activity of 1760 Kg mol_Y^{-1} h^{-1} bar^{-1}, which is classified as very high on the rating of the effectiveness of a catalyst.[54] This activity is much better than those obtained with silica-supported pentamethylcyclopentadienyl Samarium(II)[55] (64 kg_{PE} mol_{Sm}^{-1} bar^{-1} h^{-1}) which has been considered as highly active. The activity obtained is in the same range as that of a cationic zirconium metallocene catalyst supported on silica/MAO.[56] This remarkable and unprecedented performance and the transition from lab-scale to pre-industrial-scale highlighted the potential of this catalyst system designed by SOMC to significantly improve the ethylene polymerization processes.

Importantly, particle size distribution analyses were performed for selected runs and revealed spherical particles characteristic of resins generally produced via heterogeneous slurry polymerization processes (Table S2).

Conclusion

Current work aims to develop a highly active and stable olefin polymerization catalyst based on neutral and homoleptic yttrium perhydrocarbyl species supported on silica. One pursued issue with supported yttrium bis-alkyl complexes is the occurrence of a ligand transfer towards silica, resulting in a mixture of surface species. To mitigate ligand transfer, we successfully employed a sterically hindered allyl precursor, $[Y\{1,3\text{-}C_3H_3(SiMe_3)_2\}_3]$, resulting in the formation of a stable monopodal silica-supported complex, $[(\equiv SiO)Y\{\eta^3\text{-}1,3\text{-}C_3H_3(SiMe_3)_2\}_2]$, **1**, which was thoroughly characterized, including its structure studied through EXAFS investigations. Another organometallic precursor, namely $[Y(o\text{-}CH_2PhNMe_2)_3]$, was used for comparison and led to immediate ligand transfer, despite bearing a coordinating amine and primary benzylic ligand to stabilize the system.

Subsequent exploration into the resulting catalysts for ethylene polymerization revealed the exceptional activity of the monopodal species, $[(\equiv SiO)Y\{\eta^3\text{-}1,3\text{-}C_3H_3(SiMe_3)_2\}_2]$, **1**, compared to bipodal, $[(\equiv SiO)_2Y(o\text{-}CH_2PhNMe_2)]$ (80%), **2**. Unlike group 4 polymerization catalysts where an activator is required in order to obtain high activity, current system offers a high performance polymerization catalyst without any expensive and hazardous activators. Neutral catalyst **1** was implemented at a pre-industrial scale, demonstrating unprecedented activity up to 7400 $g_{PE}\cdot gcat^{-1}\cdot h^{-1}$ among supported rare-earth catalysts in presence of hydrogen or co-monomer (1-hexene). Hydrogen and 1-hexene separately show a beneficial effect with respect to the activity. However, when both are employed, the activity drops, most likely due to occurrence of side reactions.. The produced high-density polyethylenes (HDPE) exhibit a broad molar mass distribution, which is advantageous for resin processing.[2] Additionally, catalyst **1** showed good control over polymer particle morphology, rendering it suitable for polyethylene production via a slurry process.

Supporting Information

Additional DRIFT, NMR spectra, DSC and SEC figures. The authors have cited additional references within the Supporting Information.[57–60]

Acknowledgements

The authors thank INEOS for supporting this work. AdM thanks Olivier Mathon and Kiril Lomachenko for their help during the recording of the X-ray absorption spectra at ESRF, on beam line BM23. Serge Bettonville and Layane Deghedi are thanked for their valuable contribution in this project.

Keywords: supported catalyst • η^3-allyl ligand • benzyl ligand • HDPE • XAFS

[1] R. Geyer, J. R. Jambeck, K. L. Law, *Sci. Adv.* **2017**, *3*, e1700782.
[2] M. Stürzel, S. Mihan, R. Muelhaupt, *Chem. Rev.* **2016**, *116*, 1398–1433.
[3] L. Böhm, *Angew. Chem. Int. Ed.* **2003**, *42*, 5010–5030.
[4] C. Chen, *Nature Rev. Chem.* **2018**, *2*, 6–14.
[5] Y. Gao, J. Chen, Y. Wang, D. B. Pickens, A. Motta, Q. J. Wang, Y.-W. Chung, T. L. Lohr, T. J. Marks, *Nature Catal.* **2019**, *2*, 236–242.
[6] J. M. Eagan, J. Xu, R. Di Girolamo, C. M. Thurber, C. W. Macosko, A. M. LaPointe, F. S. Bates, G. W. Coates, *Science* **2017**, *355*, 814–816.
[7] M. P. McDaniel, in *Advances in Catalysis, Vol 53* (Eds.: B. Gates, H. Knozinger, F. Jentoft), **2010**, pp. 123–606.
[8] J. Severn, J. Chadwick, R. Duchateau, N. Friederichs, *Chem. Rev.* **2005**, *105*, 4073–4147.
[9] M. M. Stalzer, M. Delferro, T. J. Marks, *Catal. Lett.* **2015**, *145*, 3–14.
[10] M. C. Baier, M. A. Zuideveld, S. Mecking, *Angew. Chem. Int. Ed.* **2014**, *53*, 9722–9744.
[11] I. E. Nifant'ev, P. D. Komarov, O. D. Kostomarova, N. A. Kolosov, P. V. Ivchenko, *Polymers* **2023**, *15*, 3095.
[12] N. Popoff, J. Espinas, J. Pelletier, B. Macqueron, K. C. Szeto, O. Boyron, C. Boisson, I. Del Rosal, L. Maron, A. De Mallmann, R. M. Gauvin, M. Taoufik, *Chem. Eur. J.* **2013**, *19*, 964–973.
[13] G. Tosin, C. C. Santini, J.-M. Basset, *Top. Catal.* **2009**, *52*, 1203–1210.
[14] J. Gromada, J. Carpentier, A. Mortreux, *Coord. Chem. Rev.* **2004**, *248*, 397–410.
[15] M. K. Samantaray, E. Pump, A. Bendjeriou-Sedjerari, V. D'Elia, J. D. A. Pelletier, M. Guidotti, R. Psaro, J.-M. Basset, *Chem. Soc. Rev.* **2018**, *47*, 8403–8437.
[16] C. Coperet, A. Comas-Vives, M. P. Conley, D. P. Estes, A. Fedorov, V. Mougel, H. Nagae, F. Nunez-Zarur, P. A. Zhizhko, *Chem. Rev.* **2016**, *116*, 323–421.
[17] R. J. Witzke, A. Chapovetsky, M. P. Conley, D. M. Kaphan, M. Delferro, *ACS Catal.* **2020**, *10*, 11822–11840.
[18] R. Anwander, H. Gorlitzer, G. Gerstberger, C. Palm, O. Runte, M. Spiegler, *J. Chem. Soc. Dalton Trans.* **1999**, 3611–3615.
[19] R. M. Gauvin, L. Delevoye, R. A. Hassan, J. Keldenich, A. Mortreux, *Inorg. Chem.* **2007**, *46*, 1062–1070.
[20] Z. Wang, S. Patnaik, N. Eedugurala, J. S. Manzano, I. I. Slowing, T. Kobayashi, A. D. Sadow, M. Pruski, *J. Am. Chem. Soc.* **2020**, *142*, 2935–2947.
[21] A. G. B. Getsoian, B. Hu, J. T. Miller, A. S. Hock, *Organometallics* **2017**, *36*, 3677–3685.
[22] N. Dettenrieder, H. M. Dietrich, C. Maichle-Moessmer, R. Anwander, *Chem. Eur. J.* **2016**, *22*, 13189–13200.

[23] O. Sodpiban, S. Del Gobbo, S. Barman, V. Aomchad, P. Kidkhunthod, S. Ould-Chikh, A. Poater, V. D'Elia, J.-M. Basset, *Catal. Sci. Technol.* **2019**, *9*, 6152–6165.
[24] E. Donato, F. Medici, V. Chiroli, S. Rossi, A. Puglisi, *Tetrahedron Green Chem* **2023**, *2*, 100032.
[25] T. Vancompernolle, A. Valente, T. Chenal, P. Zinck, I. Del Rosal, L. Maron, M. Taoufik, S. Harder, R. M. Gauvin, *Organometallics* **2017**, *36*, 3912–3920.
[26] A. Mortis, C. Maichle-Mossmer, R. Anwander, *Dalton Trans.* **2022**, *51*, 1070–1085.
[27] S. Bambirra, A. Meetsma, B. Hessen, *Organometallics* **2006**, *25*, 3454–3462.
[28] P. Hitchcock, M. Lappert, R. Smith, R. Bartlett, P. Power, *J. Chem. Soc. Chem. Commun.* **1988**, 1007–1009.
[29] M. P. Conley, G. Lapadula, K. Sanders, D. Gajan, A. Lesage, I. del Rosa, L. Maron, W. W. Lukens, C. Coperet, R. A. Andersen, *J. Am. Chem. Soc.* **2016**, *138*, 3831–3843.
[30] S. C. Chmely, T. P. Hanusa, *Chem. Eur. J.* **2010**, 1321–1337.
[31] S. Harder, *Organometallics* **2005**, *24*, 373–379.
[32] T. Woodman, M. Schormann, M. Bochmann, *Isr. J. Chem.* **2002**, *42*, 283–293.
[33] M. Abrams, J. Yoder, C. Loeber, M. Day, J. Bercaw, *Organometallics* **1999**, *18*, 1389–1401.
[34] W. Evans, D. DeCoster, J. Greaves, *Organometallics* **1996**, *15*, 3210–3221.
[35] H. Sakurai, *Pure Appl. Chem.* **1982**, *54*, 1–22.
[36] J. Pelletier, J. Espinas, N. Vu, S. Norsic, A. Baudouin, L. Delevoye, J. Trebosc, E. Le Roux, C. Santini, J.-M. Basset, R. M. Gauvin, M. Taoufik, *Chem. Commun.* **2011**, *47*, 2979–2981.
[37] K. C. Szeto, Z. R. Jones, N. Merle, C. Rios, A. Gallo, F. Le Quemener, L. Delevoye, R. M. Gauvin, S. L. Scott, M. Taoufik, *ACS Catal.* **2018**, *8*, 7566–7577.
[38] G. Lapadula, A. Bourdolle, F. Allouche, M. P. Conley, I. del Rosal, L. Maron, W. W. Lukens, Y. Guyot, C. Andraud, S. Brasselet, C. Coperet, O. Maury, R. A. Andersen, *Chem. Mater.* **2014**, *26*, 1062–1073.
[39] S. Arndt, P. Voth, T. Spaniol, J. Okuda, *Organometallics* **2000**, *19*, 4690–4700.
[40] R. E. White, T. P. Hanusa, *Organometallics* **2006**, *25*, 5621–5630.
[41] M. P. McDaniel, E. D. Schwerdtfeger, M. D. Jensen, *J. Catal.* **2014**, *314*, 109–116.
[42] X. Wang, R. Salovey, *J. Appl. Polymer Sci.* **1987**, *34*, 593–599.
[43] E. Louyriac, E. Laur, A. Welle, A. Vantomme, O. Miserque, J.-M. Brusson, L. Maron, J.-F. Carpentier, E. Kirillov, *Macromolecules* **2017**, *50*, 9577–9588.
[44] C. Casey, J. Tunge, M. Fagan, *J. Org. Chem.* **2002**, *663*, 91–97.
[45] X. Kang, G. Zhou, X. Wang, J. Qu, Z. Hou, Y. Luo, *Organometallics* **2016**, *35*, 913–920.
[46] A. D. Oswald, A. El Bouhali, E. Chefdeville, P.-A. R. Breuil, H. Olivier-Bourbigou, J. Thuilliez, F. Vaultier, A. De Mallmann, M. Taoufik, L. Perrin, C. Boisson, *Organometallics* **2021**, *40*, 218–230.
[47] P. Cui, T. P. Spaniol, J. Okuda, *Organometallics* **2013**, *32*, 1176–1182.
[48] P. Cui, T. P. Spaniol, L. Maron, J. Okuda, *Chem. Eur. J.* **2013**, *19*, 13437–13444.
[49] G. Jeske, H. Lauke, H. Mauermann, P. Swepston, H. Schumann, T. Marks, *J. Am. Chem. Soc.* **1985**, *107*, 8091–8103.
[50] Y. Guan, E. Lu, X. Xu, *J. Rare Earths* **2021**, *39*, 1017–1023.
[51] C. Ehm, R. Cipullo, P. H. M. Budzelaar, V. Busico, *Dalton Trans.* **2016**, *45*, 6847–6855.
[52] G. Theurkauff, A. Bondon, V. Dorcet, J.-F. Carpentier, E. Kirillov, *Angew. Chem. Int. Ed.* **2015**, *54*, 6343–6346.
[53] A. Fischbach, R. Anwander, *Adv. Polymer Sci.* **2006**, *204*, 155–281.
[54] G. Britovsek, V. Gibson, D. Wass, *Angew. Chem. Int. Ed.* **1999**, *38*, 428–447.
[55] F. Allouche, K. W. Chan, A. Fedorov, R. A. Andersen, C. Coperet, *Angew. Chem. Int. Ed.* **2018**, *57*, 3431–3434.
[56] M. A. Bashir, V. Monteil, C. Boisson, T. F. L. McKenna, *React. Chem. Eng.* **2017**, *2*, 521–530.
[57] D. W. Sauter, V. Chiari, N. Aykac, S. Bouaouli, L. Perrin, L. Delevoye, R. M. Gauvin, K. C. Szeto, C. Boisson, M. Taoufik, *Dalton Trans.* **2017**, *46*, 11547–11551.
[58] O. Mathon, A. Beteva, J. Borrel, D. Bugnazet, S. Gatla, R. Hino, I. Kantor, T. Mairs, M. Munoz, S. Pasternak, F. Perrin, S. Pascarelli, *J. Synchrotron Radiat.* **2015**, *22*, 1548–1554.
[59] B. Ravel, M. Newville, *J. Synchrotron Radiat.* **2005**, *12*, 537–541.
[60] A. Michalowicz, J. Moscovici, D. Muller-Bouvet, K. Provost, *J. Phys. Conf.: Ser*. **2009**, *190*, 012034.

Entry for the Table of Contents

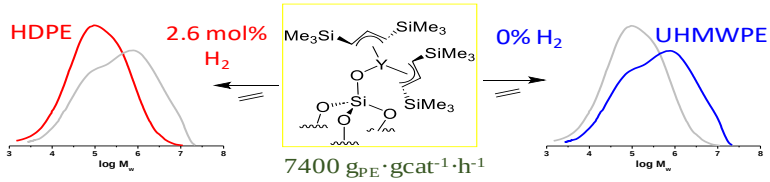

Designing of a highly active neutral yttrium supported catalyst for ethylene polymerization can be achieved by electronic and steric tuning of the ligand attached to the yttrium metal. This catalyst was implemented at a pre-industrial scale, demonstrating unprecedented activity and the desired high-density polyethylenes (HDPE) with a broad molar mass distribution, which is advantageous for resin processing.